Supplement of

Assessing the use of satellite products from multispectral unmixing and differential interferometry on Altay snow water equivalent estimation

Yiwen Fang, Jinmei Pan, Steve Margulis, Jingtian Zhou, Haorui Sun, Yang Lei, Chuan Xiong, Hua Wang, Shurun Tan*

Correspondence to: Shurun Tan (srtan@intl.zju.edu.cn)

Contents of this file

Table S1. Temporal availability of Satellite images

Water Year	Revisit times	2014	2015	2016	2017	2018	2019	2020	2021	2022	2023	2024
Landsat-8	16 days	●	●	●	●	●	●	●	●	●	●	●
Sentinel-2A	5 days			●	●	●	●	●	●	●	●	●
Sentinel-2B	5 days					●	●	●	●	●	●	●
Landsat-9	16 days									●	●	●

Table S2. Model parameters

Parameters	Distribution	Uncertainty Parameter Distributions Statistics	
Meteorological Forcings			
b (PPT)	Log normal	**Mean** 1.57	**CV** 0.53
ε_{Ta} (T_a)	Normal	**Mean** -1.40 K	**Std. Dev.** 2.58 K
ε_{Td} (T_d)	Normal	**Mean** 0.88 K	**Std. Dev.** 3.03 K
Model Parameters			
β (SDC)	Uniform	**Minimum** 0.05	**Maximum** 0.5

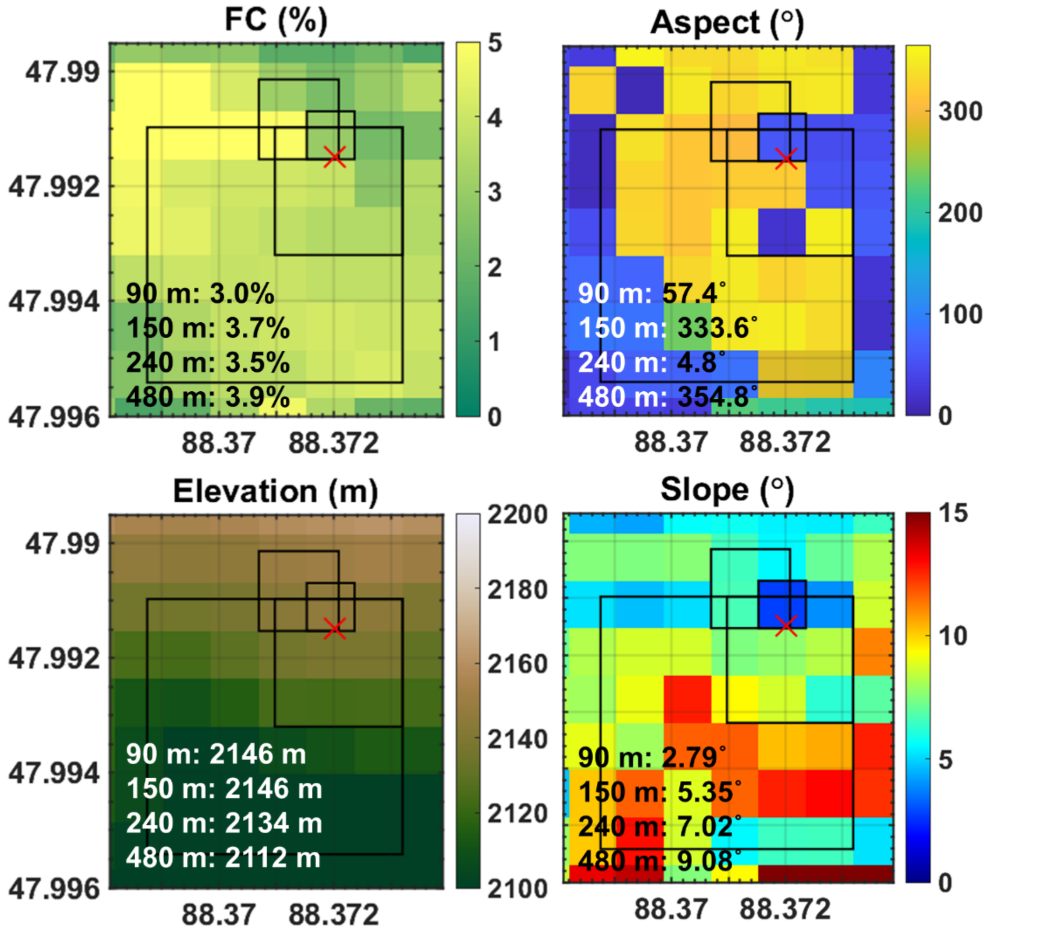

Figure S1. Forest coverage, aspect, elevation, and slope at ~90 m spatial resolution. Boxes show the boundary of ~ 90 m, 180 m, 240 m, and 480 m. The red cross sign shows the location of WXLK site.

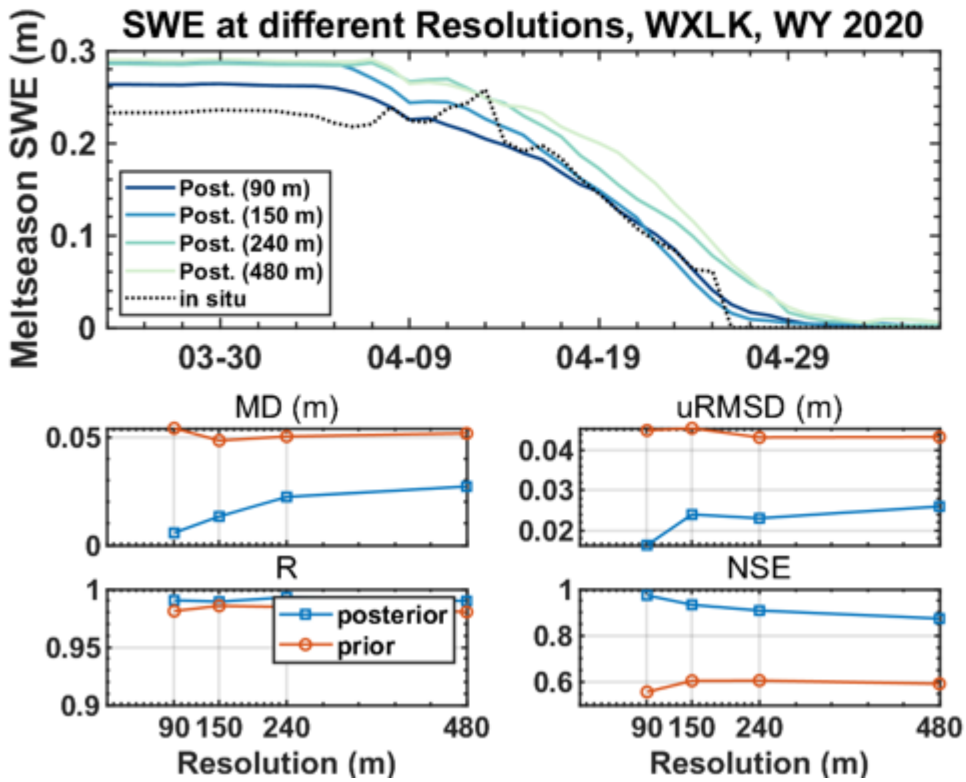

Figure S2. Time series of fSCA, SWE, and snow depth (SD) at 90 m resolution. The statistics including correlation coefficient (R), Mean Difference (MD), Root Mean Square Difference (uRMSD), Nash-Sutcliff efficiency coefficient (NSE) are summarized in the right panels for 90 m, 150m, 240 resolutions.

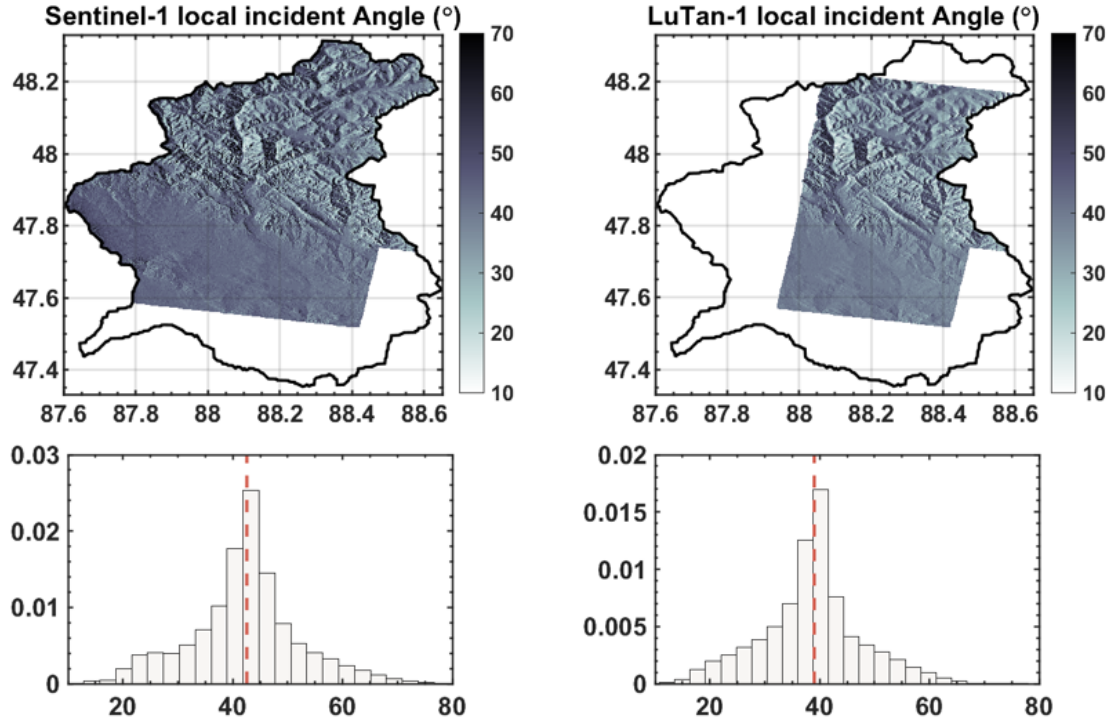

Figure S3. Local incident angles of Sentinel-1 and LuTan-1 satellites.

Text S1 Impact of fSCA products on SWE distribution

To investigate the needed number of fSCA images to constrain SWE estimates, a series of tests are conducted with the assimilation of (1) Landsat-only (L30), (2) Sentinel-only (S30), and (3) Landsat and Sentinel (HLS) fSCA in WY 2020 as shown in Fig. S4. In WY 2020, Landsat 9 has not been launched yet, therefore, L30 fSCA is retrieved from Landsat 8 alone. In this case, WXLK site only has six fSCA measurements after cloud screening in calendar year 2020. Among the 6 measurements, four of them are saturated with fSCA of 100% in the snow accumulation period, and one measurement post melt-out with fSCA of 0%. The ensemble spread at the measurement time is narrow with limited update information. There is only one fSCA measurement during snow disappearance with fSCA ~ 75%, which is slightly higher than the prior ensemble median of 72%. As a result, higher weights are assigned to ensembles with fSCA closer to 75%, pulling the posterior up towards the measurement. In this specific case, posterior SWE is not well constrained by the limited number of useful fSCA measurements from a single Landsat satellite. In contrast, Sentinel-2 A/B satellites are available in WY 2020, providing 10 fSCA measurements. There are four fSCA measurements during the melting and post melt-out season from Sentinel-2 satellites, effectively constrain the fSCA and SWE estimates. SWE generated by assimilating fSCA from Sentinel-2 satellite alone produces comparable results with assimilating both satellites yield similar posterior SWE estimates in WY 2020, 2021, and 2024 at the WXLK site. SWE generated by assimilating of Landsat fSCA alone yield higher uRMSD in WY 2020 and 2021 when only one satellite is available in contrast to comparable uRMSD in WY 2024 when two satellites are available at the WXLK site. Overall, a single satellite may not have sufficient fSCA measurements in the melting season after cloud screening. Two or more satellites with more than 10 + effective fSCA measurements are recommended to better constrain SWE.

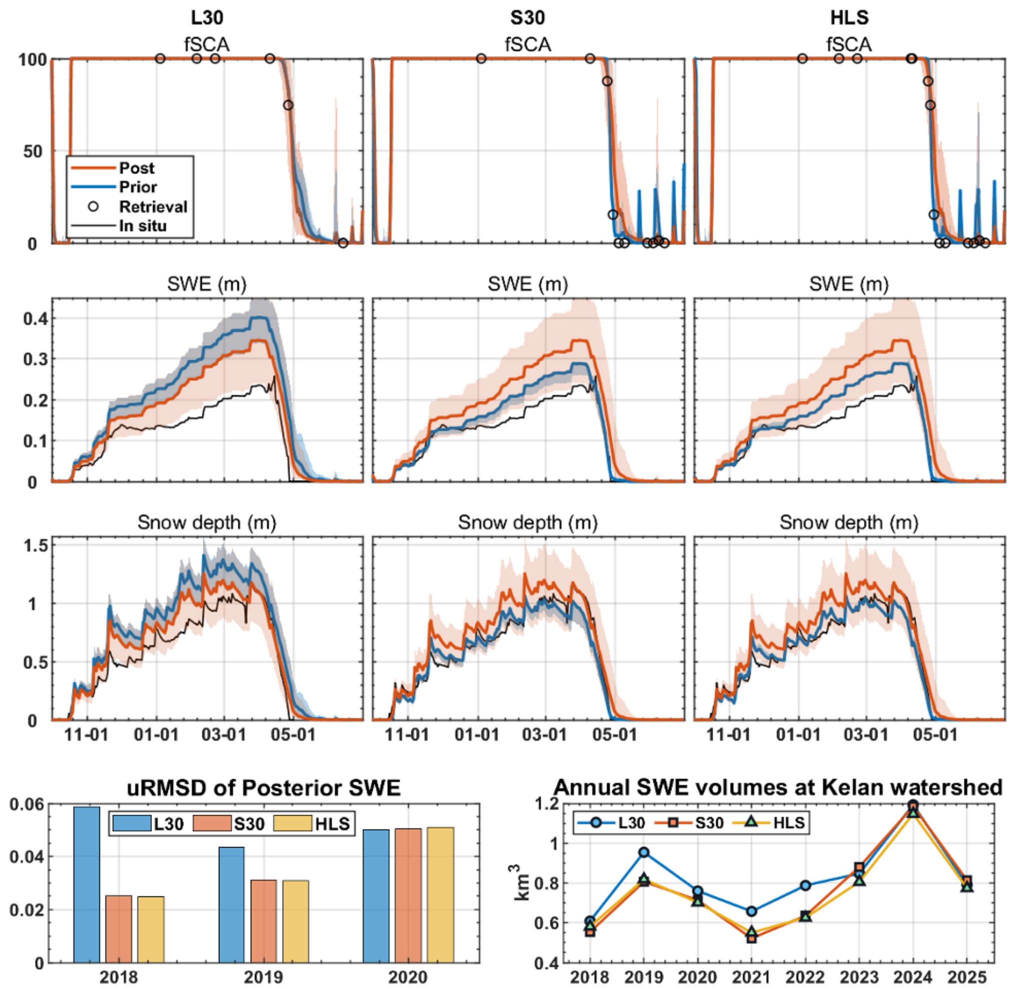

Figure S4: Time series of SWE, Snow depth, and fSCA with the assimilation of Landsat 8 (L30, left column), Sentinel-2A/2B (S30, middle column), and Harmonized Landsat Sentinel (HLS, right column, the combination of L30 and S30). Panels (a) to (c) show prior (solid red lines, open loop) and their inter-quartile range (IQR, red shades), posterior (solid blue lines, after data assimilation) and their IQR (blue shade), and in situ (black cross signs) SWE at the WXLK sites over three assimilation scenarios. Panels (d) to (f) show prior, posterior, ERA5-Land, and in situ snow depth over three scenarios. Panels (g) to (i) show prior, posterior, and retrieved HLS fSCA over three scenarios. Note that the comparison is conducted at pixel-scale rather than over the full domain. Because different random seeds are used to generate ensembles, the statistics of the results differ slightly.

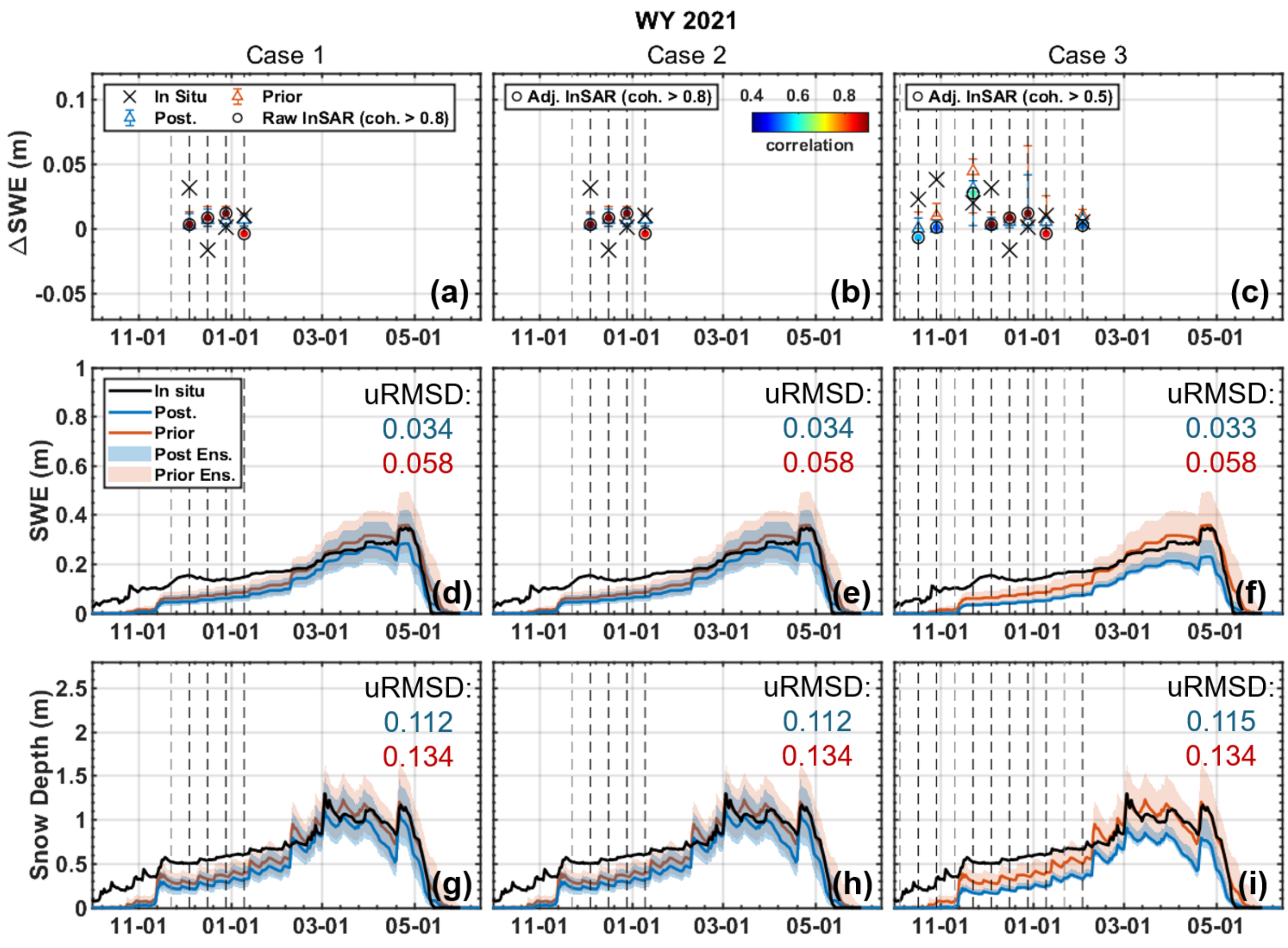

Figure S5: Time series of prior, posterior, and measured ΔSWE (a-c), SWE (d-f), and snow depth (g-i) in meters over WY 2021 at the WXLK site. ΔSWE computed from in situ SWE is marked as 'x' marks in Figure (a) and (d). Vertical dashed lines are InSAR observation dates. The left panels are results with the assimilation of all selected InSAR ΔSWE measurements. The middle panels and right panels are are results with the assimilation of adjust InSAR ΔSWE with coherence > 0.5 and 0.8, respectively.

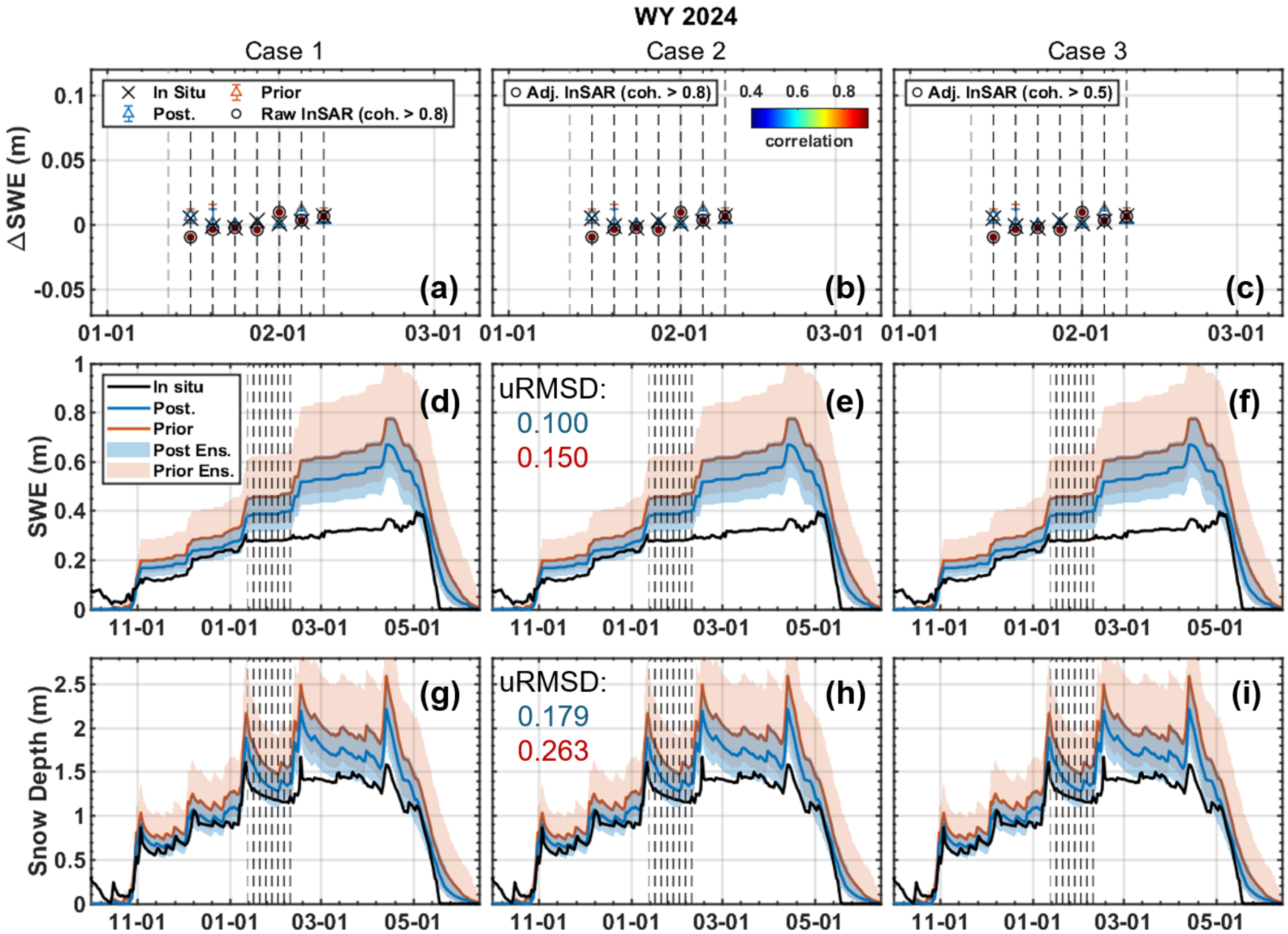

Figure S6: Same as Fig. S5 but for WY 2024. The statistics are the same for all three cases.